Large power factor, anomalous Nernst effect, and temperature-dependent thermoelectric quantum oscillations in the magnetic Weyl semimetal NdAlSi

Qing-Xin Dong,[1,3] Jin-Feng Wang,[2] Li-Bo Zhang,[1,3] Jian-Li Bai,[1,3] Qiao-Yu Liu,[1,3] Jing-Wen Cheng,[1,3] Pin-Yu Liu,[1,3] Cun-Dong Li,[1,3] Jun-Sen Xiang,[1] Zhi-An Ren,[1,3,4] Pei-Jie Sun, and Gen-Fu Chen[1,3,4,*]

[1]*Institute of Physics and Beijing National Laboratory for Condensed Matter Physics, Chinese Academy of Sciences, Beijing 100190, China*
[2]*School of Physics, Henan Province Key Laboratory of Photovoltaic Materials, Henan Normal University, Xinxiang, Henan 453007, China*
[3]*School of Physical Sciences, University of Chinese Academy of Sciences, Beijing 100049, China*
[4]*Songshan Lake Materials Laboratory, Dongguan, Guangdong 523808, China*

(Received 3 July 2023; revised 31 October 2023; accepted 1 November 2023; published 20 November 2023)

Magnetic topological materials have attracted much attention due to the interplay between magnetism and topological electronic band structure, which may not only generate new exotic quantum states but also bring great potential applications. Here, we present Seebeck and Nernst effects in the magnetic Weyl semimetal NdAlSi as a function of temperature and magnetic field. We find that the power factor reaches 15 μW cm^{-1} K^{-2} at 300 K and zero field, which compare favorably with those of traditional heavily doped semiconductors. We also find that the anomalous Nernst signals dominate the magneto-thermoelectric properties. In particular, we find that both Seebeck and Nernst effects oscillate clearly as a function of temperature in a constant magnetic field, in addition to the ordinary quantum oscillations with periodicity in inverse magnetic field at a constant temperature. Such new type of temperature-induced oscillations only appears at the narrow field-induced crossover region from a paramagnetic to a polarized paramagnetic phase and arise from the band exchange splitting due to the strong exchange interaction between conductive electrons and 4f electrons in NdAlSi. Our findings not only demonstrate the potential application of NdAlSi, but also greatly enrich the available quantum phenomena in thermoelectric response.

DOI: 10.1103/PhysRevB.108.205143

I. INTRODUCTION

Weyl semimetal (WSM) is one new type of quantum state of matter that hosts emergent fermionic quasiparticles and has initiated the great interest of scientific researchers owing to its novel phenomena and potential quantum device applications [1–5]. The typical feature of a WSM is the topologically protected linear crossings with two nondegenerate bands in the vicinity of the Fermi level, forming the Weyl nodes in pairs with opposite chirality. One common approach to generate the WSM is to break the spatial inversion symmetry in the nonmagnetic materials. Numerous materials have been found to belong to the WSM states and have been well investigated since the initial discovery in the TaAs family [3]. Another way is to search materials with time-reversal symmetry breaking, which are commonly found in various magnetic systems [6–17]. In these materials, namely, the magnetic WSMs, due to their inherent magnetic order, Berry curvature, and sensitive modifiability of the applied magnetic field, various exotic phenomena have been reported, such as topological Hall effect, the large anomalous Hall conductivity, anomalous Nernst effect, topological surface state electrochemical catalysis and giant magneto-optical responses, and so on. All of these peculiar characteristics make magnetic WSM a promising platform for potential quantum devices and stimulate researchers to explore more novel magnetic Weyl systems.

Very recently, rare-earth based RAlX compounds (R = light rare-earth elements; X = Si or Ge) with noncentrosymmetric structure have been reported to host various WSM states including type-I and/or type-II Weyl fermions by choice of R ions [12,18,19]. Notably, when the R are magnetic atoms, a simultaneous breaking of both spatial inversion and time-reversal symmetries has been realized, which is relatively rare. More importantly, the nonmagnetic reference compound (R = La) with the same crystal structure makes it convenient and intuitive to comparatively study the influence of magnetism. In such system various ground states such as magnetic glassy phase, ferromagnetic, ferrimagnetic, antiferromagnetic (AFM) and polarized paramagnetic (PPM) states, have been detected [20–27], which provides a broad platform to investigate the relationship between different magnetism and topology. Up to now, the topological characteristics of them have been investigated systematically and in depth by magneto-transport, angle-resolved photoemission spectroscopy, and first-principles calculations [12,18–26,28]. However, there are few reports on the thermoelectric transport properties of these compounds. Thermoelectric power is known as an important parameter not only for the thermoelectric energy conversion applications but also for understanding the electronic structures of materials. Specifically, quantum oscillations in Seebeck and Nernst effects, should be different from that of transport measurements, in which the oscillations

*Author to whom correspondence should be addressed: gfchen@iphy.ac.cn

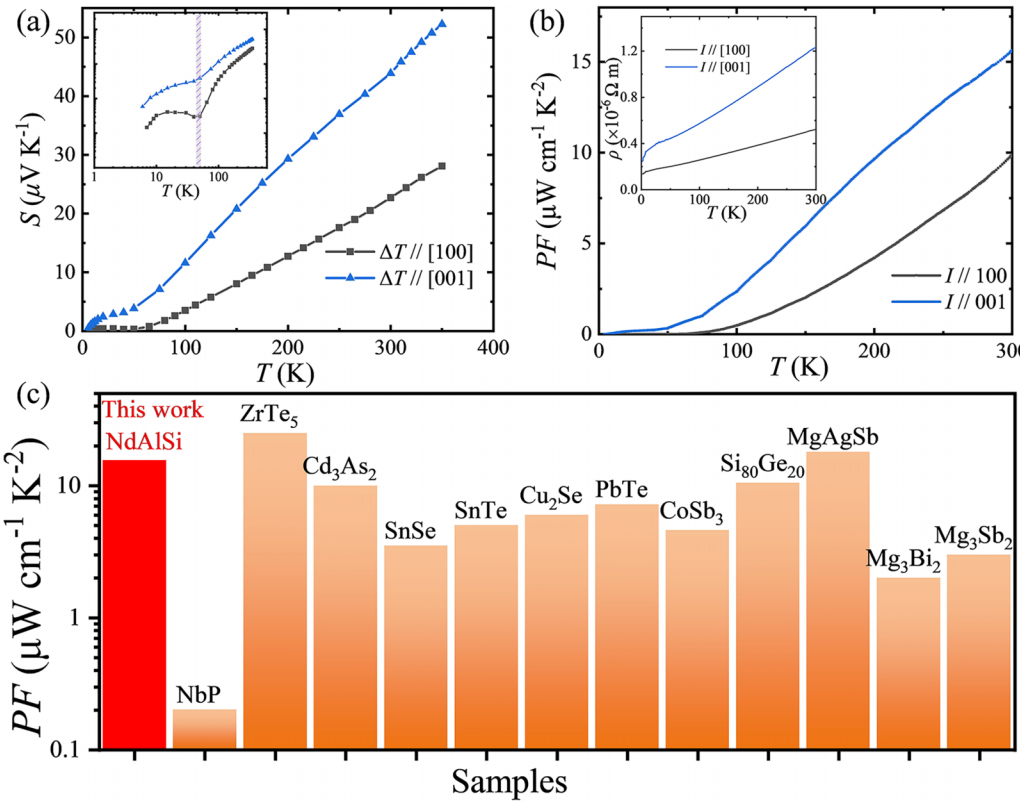

FIG. 1. (a) Seebeck coefficients as a function of temperature with current along [100] and [001] directions. Inset: the double-logarithmic coordinate is used to exhibit the abnormity of Seebeck in the low temperature. (b) Temperature dependence of power factors of NdAlSi. Inset: temperature-dependent resistivities. (c) Power factor of various topological semimetals [29–31] and high-performance thermoelectric semiconductors [32–39] at room temperature.

are directly linked to the oscillations of the density of states, while the thermoelectric quantum oscillations contain information on both transport and thermodynamic properties of the system.

In this work, we carried out the comprehensive thermoelectric transport measurements on the single crystal of NdAlSi, a magnetic Weyl semimetal candidate, which orders antiferromagnetically below 7.3 K (T_N) and could be suppressed at relatively low critical field, $B_C \sim 5.5$ T [25,27]. We find herein that a large Seebeck coefficient S, combined with rather low resistivity ρ, leads to a considerable power factor of 15 μW cm^{-1} K^{-2} at 300 K, which compares favorably with those of traditional heavily doped semiconductors. We also find that, below or above T_N, the Nernst response is dominated by the anomalous contributions, which is due to an enhanced Berry curvature from Weyl points near or at the Fermi energy in NdAlSi. All of these demonstrate the great potential of NdAlSi as a thermoelectric material. Remarkably, we find that both Seebeck and Nernst coefficients oscillate drastically not only as a function of applied magnetic field but also as a function of temperature in the cross region from paramagnetic (PM) to PPM phase for the magnetic field $H \parallel c$ axis and a heat current $\Delta T \parallel a$ axis. By contrast with LaAlSi, we attributed the novel oscillations to the destructive interference of spin-split Fermi surfaces due to the strong exchange interaction between conductive electrons and $4f$ electrons in NdAlSi. In addition, compared with the electrical magneto-transport measurements, huge quantum oscillations are found to appear in Nernst effect, indicating that the thermoelectric measurements have higher sensitivity to detecting the quantum information of materials, and which can be used as a powerful tool to probe the band structure of topological materials and explore the novel topological quantum states.

II. METHODS

High-quality single crystals of NdAlSi were grown by the self-flux method [27]. The transport and thermoelectric properties were carried out in a Quantum Design physical properties measurement system (PPMS-9 T/16 T). The Seebeck and Nernst signals were measured by using Keithley 2182 A nanovoltmeters on a self-built one-heater–two-thermometers setup with the heat current ∇T along the a axis and c axis, and the magnetic field was always perpendicular to the heat flow direction. The temperature difference was determined with field-calibrated type-E thermocouples.

III. RESULTS AND DISCUSSION

A. Large power factor

Figure 1(a) shows the temperature dependence of Seebeck coefficients $S_a(T)$ and $S_c(T)$ with the heat current ΔT parallel to the two directions, $\Delta T \parallel a$ axis and $\Delta T \parallel c$ axis, respectively, in which $S_c(T)$ is found to be much larger than that of $S_a(T)$, showing obvious anisotropy in the two directions. The positive values indicate the dominant charge carriers are holes,

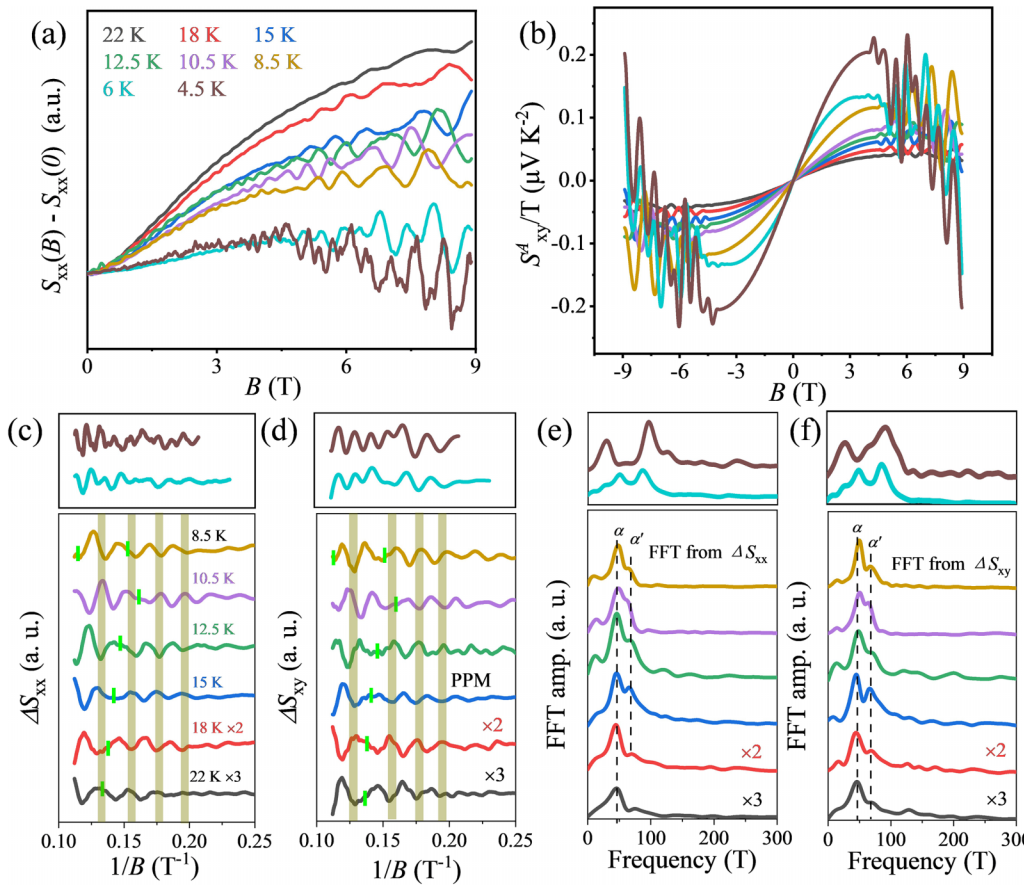

FIG. 2. (a) and (b) The magnetic field dependence of the Seebeck coefficients S_{xx} and Nernst signals S_{xy} at several selected temperatures with heat flow parallel to [100]. (c) and (d) The oscillation parts obtained from S_{xx} and S_{xy} by subtracting the smooth background. Both display a phase inversion with respect to each other. The green bars represent the node positions. (e) and (f) The FFT spectra of the S_{xx} and S_{xy} oscillation parts. Two frequencies showing no obvious temperature dependence above the T_N- are labeled as α and α'.

while $S(T)$ decreases almost linearly with temperature down to ∼50 K, consistent with the metallic behavior exhibited in the resistivity. In simple metal [40], the Seebeck coefficient can be described by $S_{xx}(T) = (\pi^2/2)\,(k_B/e)\,(k_BT/\varepsilon_F)$, where k_B and ε_F are the Boltzmann constant and Fermi level, respectively. The rough estimated values of ε_F are ∼650 meV for [100] direction and ∼350 meV for [001] direction. However, when the temperature is below 50 K, as shown in the inset of Fig. 1(a), $S(T)$ increases slightly again before it drops to zero, which is usually ascribed to the crystal-electric-field (CEF) effect or magnetic spin fluctuations as observed in many rare-earth intermetallics [41–44], which is also observed in thermal conductivity (see Fig. S3 in the Supplemental Material [45]; see also Refs. [46–49] therein). In NdAlSi, the specific heat data also suggests the CEF splitting of the tenfold degenerate Nd^{3+} $(J = 9/2)$ multiplet into a ground-state doublet and four excited doublets separated by ∼45 K [27]. Thus, the possibility that the enhancement in $S(T)$ is below 50 K is due to CEF splitting of the Nd^{3+} $(J = 9/2)$ multiplet. Remarkably, at 300 K, the moderate Seebeck coefficients coupled with extremely high electrical conductivity leads to a power factor up to 15 μW cm^{-1} K^{-2}, as displayed in Fig. 1(b), which is comparable to those of commercial topological-insulator based thermoelectric materials [32,33] and topological semimetals [29–31], as shown in the Fig. 1(c). Such an unusual thermoelectric behavior certainly merits more experimental and theoretical investigations.

B. Quantum oscillations evolving with magnetic field

Figures 2(a) and 2(b) show the magnetic field dependence of $S_{xx}(H)$ and $S_{xy}(H)$ at several selected temperatures with $\Delta T \parallel [100]$, respectively. As the magnetic field increases, quantum oscillations for magnetic fields greater than $B \sim 4$ T are clearly observed for both $S_{xx}(H)$ and $S_{xy}(H)$ with unusual temperature-dependent beating patterns instead of the usual simple $1/B$ periodic oscillations. Generally, the beating effect observed in quantum oscillations is due to the existence of two frequencies $f_\pm$ for spin-up and spin-down fermions caused by level splitting, and the position of the beating node is solely tuned by the total spin-splitting energy $\delta(B)$ coming mainly from the Zeeman spin splitting, $\Delta_Z = g\mu B$, and the spin-orbit splitting of Rashba, Δ_R. The location of the node is essentially temperature independent. As shown in the Figs. 2(c) and 2(d), however, a large shift of node positions (green bars) with temperature change in $S_{xx}(H)$ and $S_{xy}(H)$, is clearly observed in the PPM phase, while the positions of the oscillation extrema and/or minima are virtually independent of temperature [the shaded area in Figs. 2(c) and 2(d)]. Rather puzzlingly, the phase of the oscillations is inverted with temperature change,

or more precisely, the phase switches abruptly between 0 and π as a function of temperature (logarithmiclike dependence), which clearly suggests that both Zeeman and Rashba effects cannot at all account for such behaviors in this system. Up to now, such continuous phase shifts have been reported only in the magneto-transport and heat specific heat measurements in NdAlSi in a narrow field-induced crossover region from PM to PPM phase, which eventually led to the emergence of a new type of temperature-dependent quantum oscillations and has been well explained in terms of the band exchange splitting due to the strong exchange interaction between conductive electrons and $4f$ electrons [50].

To show the oscillations of $S_{xx}(H)$ and $S_{xy}(H)$ more clearly, we extract the oscillation components of them as the function of $1/B$ by subtracting the smooth background, as displayed in the Figs. 2(c) and 2(d). Clearly, the frequencies for both ΔS_{xx} and ΔS_{xy} exhibit a large shift with temperature just below T_N (see the upper panels), consistent with those observed in Shubnikov–de Haas (SdH) oscillations [50]. However, there are obvious differences for temperatures above T_N, at which the Fermi surface undergoes a sudden reconstruction [27,51]. As seen in the lower panels, the oscillations show an obvious shift of node positions and clearly invert their phase upon varying field and temperature, similar to those of the SdH oscillations in the cross region from PM to PPM phase [50]. The frequency of oscillations of S_{xx} and S_{xy} determined by taking the fast Fourier transform (FFT) are very consistent. Two frequencies are about 44 and 68 T, labeled as α and α', which show no obvious temperature dependence. According to the Onsager relation $F = (\phi_0/2\pi^2)A_F = (\hbar/2\pi e)A_F$, the frequency F is proportional to the cross-sectional area A_F of the Fermi surface normal to the field. The Fermi vector with $k_F = 0.03656$ and 0.04546 Å^{-1} and the corresponding Fermi velocity $v_F = 4.3 \times 10^5$ and 5.4×10^5 m/s and Fermi energy $E_F = 0.104$ and 0.160 derived from quantum oscillations can be obtained for Fermi surface for α and α' via $v_F = \hbar k_F/m^*$ and $E_F = m^* v_F^2$ by assuming a circular cross section.

Usually, the exchange interactions acting as an inner effective field will lead to unequal populations of spin-up and spin-down quasiparticles, and thus the cross sections of the Fermi surface differ for the two opposite-spin quasiparticles, which bring out the observed splitting of each frequency into two separate frequencies. The frequency difference ΔF between the two opposite-spin electron oscillations depends on the exchange splitting energy E_{ex} [52]. According to the literature [53], the direct exchange energy E_{ex} can be estimated from the difference between effective Fermi energies for the spin-up and spin-down components:

$$E_{ex} = \boldsymbol{J}_{\text{eff}} \cdot \boldsymbol{S} = \frac{\frac{\hbar e F_+}{m^*} - \frac{\hbar e F_-}{m^*}}{2} = \frac{\hbar e \Delta F}{2m^*},$$

where $\boldsymbol{J}_{\text{eff}}$ is the effective exchange interaction, $\boldsymbol{S}$ is the localized spins, and m^* is the effective mass ($\sim 0.1 m_e$ obtained from SdH oscillations [27]). From which we obtained E_{ex} is about 14 meV, which is comparable to the value calculated from the magneto-transport data using a simple phenomenological model that involves the magnetization behavior [50].

C. Anomalous Nernst effect

We have also carefully examined the anomalous Nernst effect, which provides us with additional useful information on the Berry curvature of the electronic states. As shown in Fig. 2(b), a large, saturated Nernst signal with a maximum about 0.2 μV K^{-2} at 9 T and 4.5 K was observed. Remarkably, the Nernst signal magnetic field dependence can be well described with the following empirical expressions [54]:

$$S_{xy} = S_{xy}^N + S_{xy}^A + S_{xy}^{OSC},$$

$$S_{xy}^N = S_0^N \frac{\mu B}{1 + (\mu B)^2},$$

$$S_{xy}^A = \Delta S_{xy}^A \tanh(B/B_0),$$

where μ is the carrier mobility, S_0^N is the amplitude of the conventional semiclassical contribution S_{xy}^N, ΔS_{xy}^A is the amplitude of the anomalous Nernst signal S_{xy}^A, B_0 is the saturation field above which the signal attains its plateau value ΔS_{xy}^A, and S_{xy}^{OSC} is the oscillating component of S_{xy}. One example of the fit at a selected temperature of 22 K is exhibited in the inset of Fig. 3(a), which reveals obviously the significant contribution of S_{xy}^A to S_{xy}. Such anomalous contributions to the thermoelectric signals have also been detected in many topological materials [11,14,17,54–56], which strongly indicate an enhanced Berry curvature from Weyl points located extremely close to the Fermi level in NdAlSi. Figure 3(a) plots the magnetic field dependent anomalous Nernst signals S_{xy}^A/T; all the curves increase monotonically at first and then show the trend toward saturation at high field with the increasing magnetic field. As the temperature rises, the amplitude ΔS_{xy}^A of the S_{xy}^A derived from the fits attenuates clearly and shows a strong temperature dependence, as shown in Fig. 3(b).

D. Quantum oscillations evolving with temperature

What is entirely unexpected, however, is the temperature dependence of $S_{xx}(T)$ and $S_{xy}(T)$ at fixed magnetic fields, as shown in Fig. 4. At low field, the $S_{xx}(T)$ does not show any abnormality. As the magnetic field increases to about 6 T and the system begins to enter the PPM state, $S_{xx}(T)$ begins to oscillate gradually as a function of temperature. As discussed in magneto-transport and heat specific heat measurements in NdAlSi, these novel temperature-dependent oscillations are also attributed to the destructive interference between quantum oscillations from the spin-split Fermi surfaces due to the strong exchange interaction between conductive electrons and $4f$ electrons. The absence of such oscillations in its sister compound with no f electrons, LaAlSi (Fig. S7), undoubtedly underscores a critical role of the $4f$ electrons of Nd. With the further increase of magnetic field, the region of oscillations is deduced and moves towards the higher temperature region. Such unconventional quantum oscillations modulated by temperature could also be understood by contrast with conventional magnetic quantum oscillations, that is, the temperature sweep causing the crossing of various Landau levels with the Fermi energy, due to the strong temperature dependence of the energies at which the Landau levels occur. These crossings may lead to successive peaks in the Seebeck and Nernst signals observed as a function of

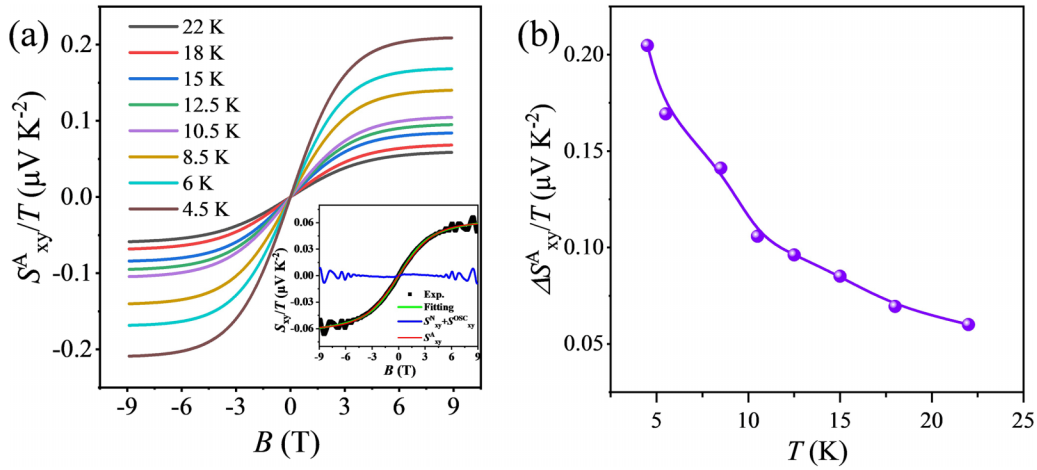

FIG. 3. (a) The magnetic field dependence of the anomalous Nernst signal S^A_{xy}/T at low temperatures. The inset exhibits the fitting result of the S_{xy} at the selected temperature of 22 K. The black and green lines represent the experimental data and fitting curve, respectively. The red line is the anomalous component of S_{xy} and the blue line is the sum contribution from the normal Nernst signal S^N_{xy} and the oscillating component S^{OSC}_{xy}. (b) The temperature dependence of the amplitude of anomalous Nernst signal $\Delta S^A_{xy}/T$.

temperature, similar to those observed in the usual magneto-thermal oscillations by sweeping the magnetic field at a fixed temperature.

Figure 4(b) reveals the temperature-dependent $S_{xy}(T)$ at several selected magnetic fields. Similar to the $S_{xx}(T)$, with the increase of magnetic field, the region of oscillations on $S_{xy}(T)$ is also deduced and moves towards the higher temperature region. However, there is some difference that the $S_{xy}(T)$ begins to oscillate with the temperature at about 3 T, which is close to the critical magnetic field of the polarized paramagnetic ground state obtained from the resistivity and specific heat [50], indicating that the polarization occurs before the suppression of AFM order. In addition, it is worth noting that the $S_{xy}(T)$ has a larger amplitude of oscillation than that of $S_{xx}(T)$ at the same magnetic field. For a clearer comparison, we plot the $\Delta S_{xx}(T)$ and $\Delta S_{xy}(T)$ together at selected magnetic fields 9 and 16 T, as shown in Fig. 4(c). One can see obviously that the amplitude of $\Delta S_{xy}(T)$ is three to five times larger than that of $\Delta S_{xx}(T)$, suggesting that the Nernst signal is more sensitive to electronic states and could be used as an important probe to study the band structure of topological materials and explore the novel topological quantum state.

IV. CONCLUSION

In summary, we systematically investigated the thermoelectric transport properties of the magnetic Weyl semimetal NdAlSi. The large Seebeck coefficient and very low resistivity enable a large power factor in NdAlSi. Remarkably, a large anomalous Nernst signal, as direct evidence of a large Berry curvature from Weyl points near or at the Fermi energy, was also clearly observed below and above the magnetic transition temperature. Furthermore, both Seebeck and Nernst signal oscillations occur as a function of temperature in a fixed magnetic field above 3 T, while the non-f reference compound LaAlSi does not. All these unique features not only demonstrate the great potential of NdAlSi as a thermoelectric material, but also provide thermodynamic evidence that the unique temperature-dependent quantum oscillations

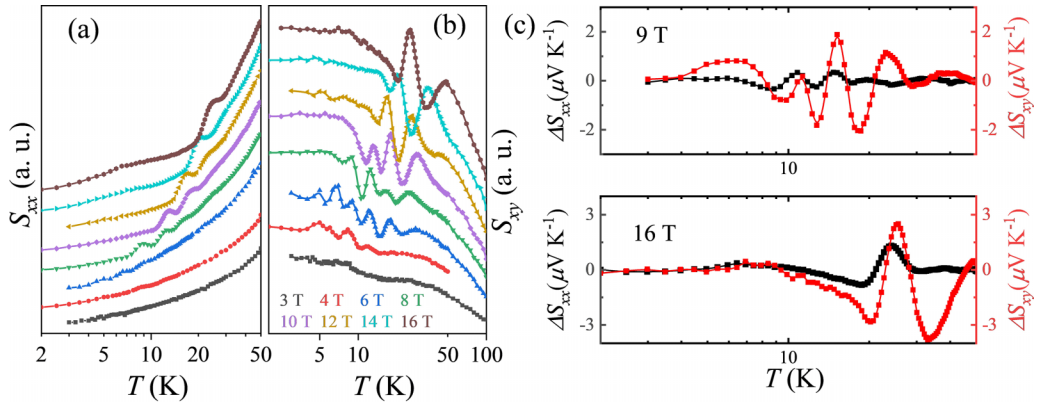

FIG. 4. The temperature-dependent (a) S_{xx} and (b) S_{xy} of NdAlSi at several selected magnetic fields. Both exhibit the obvious oscillations as a function of temperature. (c) The comparison of ΔS_{xx} with ΔS_{xy} at selected magnetic fields. ΔS_{xy} shows a larger amplitude than that of ΔS_{xx}.

are associated with the strong exchange interaction between conductive electrons and $4f$ electrons, as previously observed on the magneto-transport and specific heat measurements. Our findings not only reveal the potential application of NdAlSi, but also greatly enrich the quantum phenomena in thermoelectric response, which further permit the exploration of new novel topological quantum states emerging from the effective coupling between conduction electrons and the magnetic moments of $3d$ and/or $4f$ ions in magnetic topological materials.

ACKNOWLEDGMENTS

This work was supported by the National Natural Science Foundation of China (Grant No. 12274440), the Strategic Priority Research Program (B) of Chinese Academy of Sciences (Grant No. XDB33010100), the Ministry of Science and Technology of China (Grant No. 2022YFA1403903) and Henan Center for Outstanding Overseas Scientists (No. GZS2023007), and the Synergetic Extreme Condition User Facility (SECUF).

Q.-X.D. and J.-F.W. contributed equally to this work.

[1] N. P. Armitage, E. J. Mele, and A. Vishwanath, Weyl and Dirac semimetals in three-dimensional solids, Rev. Mod. Phys. **90**, 015001 (2018).

[2] H. Weng, C. Fang, Z. Fang, B. A. Bernevig, and X. Dai, Weyl semimetal phase in noncentrosymmetric transition-metal monophosphides, Phys. Rev. X **5**, 011029 (2015).

[3] X. Huang, L. Zhao, Y. Long, P. Wang, D. Chen, Z. Yang, H. Liang, M. Xue, H. Weng, Z. Fang *et al.*, Observation of the chiral-anomaly-induced negative magnetoresistance in 3D Weyl semimetal TaAs, Phys. Rev. X **5**, 031023 (2015).

[4] B. Yan and C. Felser, Topological materials: Weyl semimetals, Annu. Rev. Condens. Matter Phys. **8**, 337 (2017).

[5] K. Manna, Y. Sun, L. Muechler, J. Kübler, and C. Felser, Heusler, Weyl and Berry, Nat. Rev. Mater. **3**, 244 (2018).

[6] S. N. Guin, P. Vir, Y. Zhang, N. Kumar, S. J. Watzman, C. Fu, E. Liu, K. Manna, W. Schnelle, and J. Gooth *et al.*, Zero-field Nernst effect in a ferromagnetic kagome-lattice Weyl-semimetal $Co_3Sn_2S_2$, Adv. Mater. **31**, 1806622 (2019).

[7] E. Liu, Y. Sun, N. Kumar, L. Muechler, A. Sun, L. Jiao, S.-Y. Yang, D. Liu, A. Liang, Q. Xu *et al.*, Giant anomalous Hall effect in a ferromagnetic kagome-lattice semimetal, Nat. Phys. **14**, 1125 (2018).

[8] Y. Okamura, S. Minami, Y. Kato, Y. Fujishiro, Y. Kaneko, J. Ikeda, J. Muramoto, R. Kaneko, K. Ueda, V. Kocsis *et al.*, Giant magneto-optical responses in magnetic Weyl semimetal $Co_3Sn_2S_2$, Nat. Commun. **11**, 4619 (2020).

[9] K. Kuroda, T. Tomita, M.-T. Suzuki, C. Bareille, A. A. Nugroho, P. Goswami, M. Ochi, M. Ikhlas, M. Nakayama, S. Akebi *et al.*, Evidence for magnetic Weyl fermions in a correlated metal, Nat. Mater. **16**, 1090 (2017).

[10] K. Kim, J. Seo, E. Lee, K.-T. Ko, B. S. Kim, B. G. Jang, J. M. Ok, J. Lee, Y. J. Jo, W. Kang *et al.*, Large anomalous Hall current induced by topological nodal lines in a ferromagnetic van der Waals semimetal, Nat. Mater. **17**, 794 (2018).

[11] J. Xu, W. A. Phelan, and C.-L. Chien, Large anomalous Nernst effect in a van der Waals ferromagnet Fe_3GeTe_2, Nano Lett. **19**, 8250 (2019).

[12] D. S. Sanchez, G. Chang, I. Belopolski, H. Lu, J.-X. Yin, N. Alidoust, X. Xu, T. A. Cochran, X. Zhang, Y. Bian *et al.*, Observation of Weyl fermions in a magnetic non-centrosymmetric crystal, Nat. Commun. **11**, 3356 (2020).

[13] Y. Zhang, Y. Yin, G. Dubuis, T. Butler, N. V. Medhekar, and S. Granville, Berry curvature origin of the thickness-dependent anomalous Hall effect in a ferromagnetic Weyl semimetal, npj Quantum Mater. **6**, 17 (2021).

[14] H. Zhang, C. Q. Xu, and X. Ke, Topological Nernst effect, anomalous Nernst effect, and anomalous thermal Hall effect in the Dirac semimetal Fe_3Sn_2, Phys. Rev. B **103**, L201101 (2021).

[15] H. Li, B. Ding, J. Chen, Z. Li, Z. Hou, E. Liu, H. Zhang, X. Xi, G. Wu, and W. Wang, Large topological Hall effect in a geometrically frustrated kagome magnet Fe_3Sn_2, Appl. Phys. Lett. **114**, 192408 (2019).

[16] Y. Deng, Y. Yu, M. Z. Shi, Z. Guo, Z. Xu, J. Wang, X. H. Chen, and Y. Zhang, Quantum anomalous Hall effect in intrinsic magnetic topological insulator $MnBi_2Te_4$, Science **367**, 895 (2020).

[17] A. Sakai, Y. P. Mizuta, A. A. Nugroho, R. Sihombing, T. Koretsune, M.-T. Suzuki, N. Takemori, R. Ishii, D. Nishio-Hamane, R. Arita *et al.*, Giant anomalous Nernst effect and quantum-critical scaling in a ferromagnetic semimetal, Nat. Phys. **14**, 1119 (2018).

[18] G. Chang, B. Singh, S.-Y. Xu, G. Bian, S.-M. Huang, C.-H. Hsu, I. Belopolski, N. Alidoust, D. S. Sanchez, H. Zheng *et al.*, Magnetic and noncentrosymmetric Weyl fermion semimetals in the RAlGe family of compounds (R = rare earth), Phys. Rev. B **97**, 041104(R) (2018).

[19] S.-Y. Xu, N. Alidoust, G. Chang, H. Lu, B. Singh, I. Belopolski, D. S. Sanchez, X. Zhang, G. Bian, and H. Zheng, Discovery of Lorentz-violating type II Weyl fermions in LaAlGe, Sci. Adv. **3**, e1603266 (2017).

[20] J. Zhao, W. Liu, A. Rahman, F. Meng, L. Ling, C. Xi, W. Tong, Y. Bai, Z. Tian, and Y. Zhong, Field-induced tricritical phenomenon and magnetic structures in magnetic Weyl semimetal candidate NdAlGe, New J. Phys. **24**, 013010 (2022).

[21] P. Puphal, V. Pomjakushin, N. Kanazawa, V. Ukleev, D. J. Gawryluk, J. Ma, M. Naamneh, N. C. Plumb, L. Keller, R. Cubitt *et al.*, Topological magnetic phase in the candidate Weyl semimetal CeAlGe, Phys. Rev. Lett. **124**, 017202 (2020).

[22] M. M. Piva, J. C. Souza, V. Brousseau-Couture, S. Sorn, K. R. Pakuszewski, J. K. John, C. Adriano, M. Côté, P. G. Pagliuso, A. Paramekanti *et al.*, Topological features in the ferromagnetic Weyl semimetal CeAlSi: Role of domain walls, Phys. Rev. Res. **5**, 013068 (2023).

[23] Y. Sun, C. Lee, H.-Y. Yang, D. H. Torchinsky, F. Tafti, and J. Orenstein, Mapping domain-wall topology in the magnetic Weyl semimetal CeAlSi, Phys. Rev. B **104**, 235119 (2021).

[24] L. Wu, S. Chi, H. Zuo, G. Xu, L. Zhao, Y. Luo, and Z. Zhu, Field-induced Lifshitz transition in the magnetic Weyl semimetal candidate PrAlSi, npj Quantum Mater. **8**, 4 (2023).

[25] J. Gaudet, H.-Y. Yang, S. Baidya, B. Lu, G. Xu, Y. Zhao, J. A. Rodriguez-Rivera, C. M. Hoffmann, D. E. Graf, D. H. Torchinsky *et al.*, Weyl-mediated helical magnetism in NdAlSi, Nat. Mater. **20**, 1650 (2021).

[26] X. Yao, J. Gaudet, R. Verma, D. E. Graf, H.-Y. Yang, F. Bahrami, R. Zhang, A. A. Aczel, S. Subedi, D. H. Torchinsky *et al.*, Large topological Hall effect and spiral magnetic order in the Weyl semimetal SmAlSi, Phys. Rev. X **13**, 011035 (2023).

[27] J.-F. Wang, Q.-X. Dong, Z.-P. Guo, M. Lv, Y.-F. Huang, J.-S. Xiang, Z.-A. Ren, Z.-J. Wang, P.-J. Sun, and G. Li, NdAlSi: A magnetic Weyl semimetal candidate with rich magnetic phases and atypical transport properties, Phys. Rev. B **105**, 144435 (2022).

[28] H. Su, X. Shi, J. Yuan, Y. Wan, E. Cheng, C. Xi, L. Pi, X. Wang, Z. Zou, N. Yu *et al.*, Multiple Weyl fermions in the non-centrosymmetric semimetal LaAlSi, Phys. Rev. B **103**, 165128 (2021).

[29] C. Fu, S. N. Guin, S. J. Watzman, G. Li, E. Liu, N. Kumar, V. Süß, W. Schnelle, G. Auffermann, C. Shekhar *et al.*, Large Nernst power factor over a broad temperature range in polycrystalline Weyl semimetal NbP, Energy Environ. Sci. **11**, 2813 (2018).

[30] P. Wang, C.-w. Cho, F. Tang, P. Wang, W. Zhang, M. He, G. Gu, X. Wu, Y. Shao, and L. Zhang, Giant Nernst effect and field-enhanced transversal $z_N T$ in $ZrTe_5$, Phys. Rev. B **103**, 045203 (2021).

[31] J. S. Xiang, S. L. Hu, M. Lyu, W. L. Zhu, C. Y. Ma, Z. Y. Chen, F. Steglich, G. F. Chen, and P. J. Sun, Large transverse thermoelectric figure of merit in a topological Dirac semimetal, Sci. China: Phys., Mech. Astron. **63**, 1 (2020).

[32] X. Mo, J. Liao, G. Yuan, S. Zhu, X. Lei, L. Huang, Q. Zhang, C. Wang, and Z. Ren, High thermoelectric performance at room temperature of n-type Mg_3Bi_2-based materials by Se doping, J. Magnesium Alloys **10**, 1024 (2022).

[33] Z. Ren, J. Shuai, J. Mao, Q. Zhu, S. Song, Y. Ni, and S. Chen, Significantly enhanced thermoelectric properties of p-type Mg_3Sb_2 via co-doping of Na and Zn, Acta Mater. **143**, 265 (2018).

[34] Y. Z. Pei, X. Y. Shi, A. LaLonde, H. Wang, L. D. Chen, and G. J. Snyder, Convergence of electronic bands for high performance bulk thermoelectrics, Nature (London) **473**, 66 (2011).

[35] L. D. Zhao, S. H. Lo, Y. S. Zhang, H. Sun, G. J. Tan, C. Uher, C. Wolverton, V. P. Dravid, and M. G. Kanatzidis, Ultralow thermal conductivity and high thermoelectric figure of merit in SnSe crystals, Nature (London) **508**, 373 (2014).

[36] Z. Zhang, K. Zhao, T.-R. Wei, P. Qiu, L. Chen, and X. Shi, Cu_2Se-based liquid-like thermoelectric materials: Looking back and stepping forward, Energy Environ. Sci. **13**, 3307 (2020).

[37] Y. Tang, Z. M. Gibbs, L. A. Agapito, G. Li, H.-S. Kim, B. Nardelli, S. Curtarolo Marco, and G. J. Snyder, Convergence of multi-valley bands as the electronic origin of high thermoelectric performance in $CoSb_3$ skutterudites, Nat. Mater. **14**, 1223 (2015).

[38] G. Joshi, H. Lee, Y. Lan, X. Wang, G. Zhu, D. Wang, R. W. Gould, D. C. Cuff, M. Y. Tang, M. S. Dresselhaus *et al.*, Enhanced thermoelectric figure-of-merit in nanostructured p-type silicon germanium bulk alloys, Nano Lett. **8**, 4670 (2008).

[39] H. Zhao, J. Sui, Z. Tang, Y. Lan, Q. Jie, D. Kraemer, K. McEnaney, A. Guloy, G. Chen, and Z. Ren, High thermoelectric performance of MgAgSb-based materials, Nano Energy **7**, 97 (2014).

[40] K. Behnia, *Fundamentals of Thermoelectricity* (Oxford University Press, Oxford, 2015), Chap. 5.

[41] D. T. Adroja, B. D. Padalia, S. N. Bhatia, and S. K. Malik, Thermoelectric power of the Kondo-lattice system: CePdSn, Phys. Rev. B **45**, 477 (1992).

[42] E. Bauer, S. Berger, C. Paul, M. D. Mea, G. Hilscher, H. Michor, M. Reissner, W. Steiner, A. Grytsiv, P. Rogl *et al.*, Crystal field effects and thermoelectric properties of $PrFe_4Sb_{12}$ skutterudite, Phys. Rev. B **66**, 214421 (2002).

[43] T. Toliński, Crystal electric field contribution to the thermoelectric power of the $CeCoAl_4$ antiferromagnetic, Int. J. Mod Phys B **32**, 1850347 (2018).

[44] N. Oeschler, S. Hartmann, U. Köhler, M. Deppe, P. Sun, and F. Steglich, Thermoelectric Power of Correlated Compounds, in *NATO Science for Peace and Security Series B: Physics and Biophysics* (Springer, Netherlands, 2009), pp. 81.

[45] See Supplemental Material at http://link.aps.org/supplemental/10.1103/PhysRevB.108.205143 for information on thermal conductivity and references therein.

[46] R. Jin, Y. Onose, Y. Tokura, D. Mandrus, P. Dai, and B. Sales, In-plane thermal conductivity of Nd_2CuO_4: Evidence for magnon heat transport, Phys. Rev. Lett. **91**, 146601 (2003).

[47] J. Takeya, I. Tsukada, Y. Ando, T. Masuda, and K. Uchinokura, Thermal conductivity of Mg-doped $CuGeO_3$ at very low temperatures: Heat conduction by antiferromagnetic magnons, Phys. Rev. B **62**, R9260(R) (2000).

[48] L. Chen, R. Liu, and X. Shi, *Thermoelectric Materials and Devices* (Elsevier, New York, 2020).

[49] T. Liang, Q. Gibson, J. Xiong, M. Hirschberger, S. P. Koduvayur, R. J. Cava, and N. P. Ong, Evidence for massive bulk Dirac fermions in $Pb_{1-x}Sn_xSe$ from Nernst and thermopower experiments, Nat. Commun. **4**, 2696 (2013).

[50] J.-F. Wang, Q.-X. Dong, Y.-F. Huang, Z.-S. Wang, Z.-P. Guo, Z.-J. Wang, Z.-A. Ren, G. Li, P.-J. Sun, X. Dai *et al.*, Quantum oscillations in the magnetic Weyl semimetal NdAlSi arising from strong Weyl fermion—4*f* electron exchange interaction, Phys. Rev. B **108**, 024423 (2023).

[51] N. Zhang, X. Ding, F. Zhan, H. Li, H. Li, K. Tang, Y. Qian, S. Pan, X. Xiao, J. Zhang *et al.*, Temperature-dependent and magnetism-controlled Fermi surface changes in magnetic Weyl semimetals, Phys. Rev. Res. **5**, L022013 (2023).

[52] M. Springford, *Electrons at the Fermi Surface* (Cambridge University Press, Cambridge, UK, 2011).

[53] R. Goodrich, N. Harrison, and Z. Fisk, Fermi surface changes across the Néel phase boundary of NdB_6, Phys. Rev. Lett. **97**, 146404 (2006).

[54] T. Liang, J. Lin, Q. Gibson, T. Gao, M. Hirschberger, M. Liu, R. J. Cava, and N. P. Ong, Anomalous Nernst effect in the Dirac semimetal Cd_3As_2, Phys. Rev. Lett. **118**, 136601 (2017).

[55] S. N. Guin, K. Manna, J. Noky, S. J. Watzman, C. Fu, N. Kumar, W. Schnelle, C. Shekhar, Y. Sun, and J. Gooth, Anomalous Nernst effect beyond the magnetization scaling relation in the ferromagnetic Heusler compound Co_2MnGa, NPG Asia Mater. **11**, 16 (2019).

[56] X. Li, L. Xu, L. Ding, J. Wang, M. Shen, X. Lu, Z. Zhu, and K. Behnia, Anomalous Nernst and Righi-Leduc effects in Mn_3Sn: Berry curvature and entropy flow, Phys. Rev. Lett. **119**, 056601 (2017).